Experiments in Fluids (2005) 39: 75–85
DOI 10.1007/s00348-005-0979-3

ORIGINALS

M. M. Zhang · Y. Zhou · L. Cheng

Closed-loop-manipulated wake of a stationary square cylinder

Received: 20 February 2004 / Revised: 9 March 2005 / Accepted: 9 March 2005 / Published online: 14 May 2005

Abstract Vortex shedding from a fixed rigid square cylinder in a cross flow was manipulated by perturbing the cylinder surface using piezo-ceramic actuators, which were activated by a feedback hot-wire signal via a proportional–integral–derivative (PID) controller. The manipulated flow was measured at a Reynolds number (*Re*) of 7,400 using particle image velocimetry (PIV), laser-induced fluorescence (LIF) flow visualisation, two-component laser Doppler anemometry (LDA), hot wires and load cells. It is observed that the vortex circulation, fluctuating streamwise velocity, lift and drag coefficients and mean drag coefficient may decrease by 71%, 40%, 51%, 42% and 20%, respectively, compared with the unperturbed flow, if the perturbation velocity of the cylinder surface is anti-phased with the flow lateral velocity associated with vortex shedding. On the other hand, these quantities may increase by 152%, 90%, 60%, 67% and 37%, respectively, given in-phased cylinder surface perturbation and vortex shedding. Similar effects are obtained at $Re = 3{,}200$ and 9,500, respectively. The relationship between the perturbation and flow modification is examined, which provides insight into the physics behind the observation.

1 Introduction

The turbulent wake of a bluff body is frequently seen in engineering. Its control is of both fundamental and engineering significance. Various techniques have been proposed, among which, closed-loop controls use the system response as feedback signals to activate actuators via controllers and have become a hot topic in the past decade (Gad-el-Hak 2001). Most previous investigations aimed at suppressing unsteady flow or flow-induced structural vibration, including Berger (1967), Williams and Zhao (1989), Baz and Ro (1991), Tokumaru and Dimotakis (1991), Roussopoulos (1993), Huang (1996) and Warui and Fujisawa (1996). Others, such as Turner et al. (1993), Tsutsui et al. (2001) and Wang et al. (2003), were interested in reinforcing unsteady wake for transport enhancement in heat transfer or combustion applications.

The actuation mechanism is an important component in an active flow control system. Frequently used mechanisms include acoustic excitation, moving cylinders and surface bleeding. Cheng et al. (2003) recently proposed a novel technique to attenuate the resonant fluid–structure interaction. The essence of the technique is to create a perturbation on the surface of a bluff body using piezo-ceramic actuators, which alters interactions between vortex shedding and structural vibration from synchronising to moving against each other. Using an open-loop scheme and a spring-supported square cylinder, Zhang et al. (2003) showed that both the structural vibration and the strength of vortices were greatly enhanced when f_p^* ($=f_p h/U_\infty$, where U_∞ is the free-stream velocity, f_p is the perturbation frequency and h is the height of the cylinder) fell in the synchronisation range ($0.11 < f_p^* < 0.26$), but were otherwise impaired. The control effect was significantly improved once a closed-loop control was introduced (Zhang et al. 2004a). Zhang et al. (2004b) found that the performance of a closed-loop control system strongly depended upon the feedback signal used. The system performed best when a combination of hot wire and structural vibration signals, rather than either a hot wire or a structural vibration signal, was used as the feedback signal.

The aforementioned work based on perturbing the cylinder surface was entirely conducted in the context of a flexibly supported cylinder. As such, the

M. M. Zhang · Y. Zhou · L. Cheng (✉)
Department of Mechanical Engineering,
The Hong Kong Polytechnic University,
Hung Hom, Kowloon, Hong Kong
E-mail: mmlcheng@polyu.edu.hk
Tel.: +852-27666769
Fax: +852-23654703

vortex-induced structural oscillation was rather significant, up to 0.08h (h is the cylinder height) at the occurrence of resonance, where the frequency of vortex shedding coincided with the natural frequency of the fluid–structure system. It has been seen that the oscillation, under the closed-loop-controlled perturbation, was turned into anti-phase with vortex shedding and, accordingly, almost completely destroyed the vortex street (Zhang et al. 2004b). Since the surface perturbation amplitude used was typically 7% of the structural oscillation, it was technically difficult to disassociate the perturbation from the oscillation of the whole structure in terms of the role played in modifying the flow so as to extract the intrinsic relationship between the perturbation and the flow field. This relationship is believed to be crucial in fully understanding the control mechanism. Furthermore, in the absence of significant structural oscillation, one wonders whether such a surface perturbation technique is still effective in the flow control.

This work aims to address the aforementioned two issues. A fixed rigid square cylinder was used. The test model was built with piezo-ceramic actuators to perturb the cylinder surface, along with a closed-loop control system deploying a simplified proportional–integral–derivative (PID) controller. Tuned at one Reynolds number ($Re = U_\infty h/\nu$, where ν is the kinematic viscosity), the effectiveness of the controller was assessed in a range of Re to examine its robustness. The flow behind the cylinder was documented using a number of techniques, including particle image velocimetry (PIV), laser-induced fluorescence (LIF) flow visualisation, laser Doppler anemometry (LDA) and hot-wire velocimetry. The fluctuating lift and drag forces on the cylinder were measured using load cells. The cylinder surface perturbation was monitored using a laser vibrometer simultaneously with the forces or flow, thus, allowing the relationship between the perturbation and flow modification to be examined in detail.

2 Experimental condition

Experiments were conducted in a closed-circuit wind tunnel with a working section of 2.0×0.6×0.6 m. Details of the tunnel were given in Zhou et al. (2002). A square cylinder made of aluminum alloy, with a height $h = 16.1$ mm, was horizontally fixed at both ends on the sidewalls of the wind tunnel (Fig. 1). Three curved piezo-ceramic actuators (THUNDER-8R) were embedded in series on the upper side of the cylinder and covered with a 13.8×493-mm plastic plate of 3-mm thickness, which was flush with the remaining part of the cylinder surface. Driven by the actuators, this plate may oscillate up and down to create a perturbation to the flow on the cylinder surface. The properties of the actuators, depending on the installation detail, were described in Cheng et al. (2003) and Marouze and Cheng (2002). Typically, without any loading, the presently used actuators may vibrate at a frequency bandwidth up to 2 kHz and with a maximum displacement of about 2 mm. The possible oscillation in the in-line direction was measured at different spanwise locations on the cylinder using a laser vibrometer, which was negligibly small, regardless of the actuation.

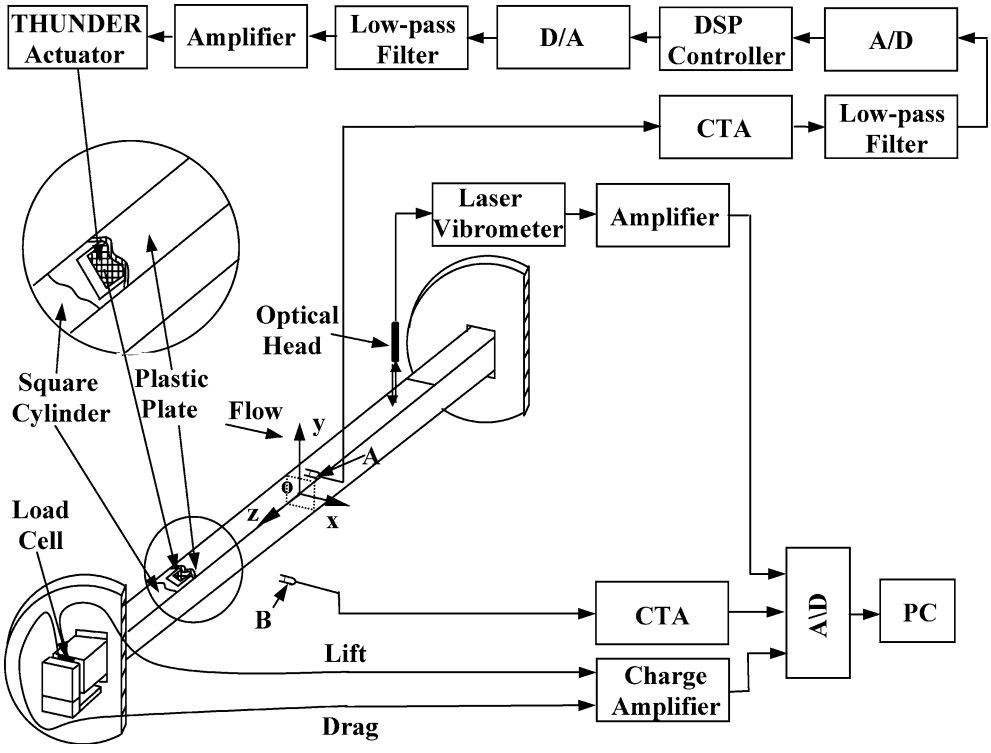

Fig. 1 Experimental setup. Feedback and monitoring hot wires A and B were placed at $x/h = 0$, $y/h = 1.6$, $z/h = 0$ and at $x/h = 2$, $y/h = 1.5$, $z/h = 4$, respectively

Hot wire A, made of a 5-μm tungsten wire, measured the streamwise fluctuating velocity (u), which was used as the feedback signal for the control system. The wire was placed at $x/h=0$, $y/h=1.6$ and $z/h=0$, where x, y and z are the streamwise, transverse and spanwise direction coordinates, respectively, with the origin defined at the cylinder centre (Fig. 1). At this location, a clean signal of vortex shedding was detected and the system delay due to the dislocation between the sensor and actuators was reduced to a minimum. After amplification, the feedback signal was processed through a low-pass filter at a cutoff frequency of 200 Hz to a digital signal processor (DSP) controller fitted with 16-bit AD and DA converters. The converted analogue signal was low-pass filtered again at a cutoff frequency of 200 Hz and amplified by two dual-channel piezo-driver amplifiers (Trek PZD 700) to activate the actuators. The use of the two low-pass filters for both the feedforward and feedback passages was to remove high-frequency noises from turbulence and electronic components.

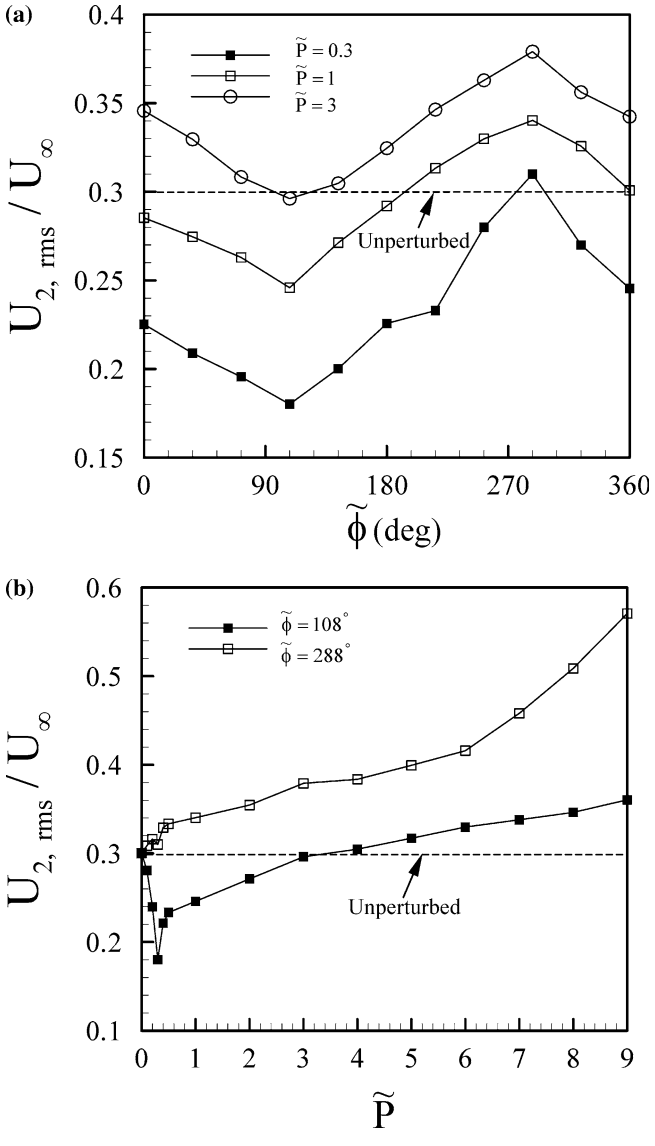

Fig. 2 Dependence of $u_{2,\mathrm{rms}}$ on **a** phase shift $\left(\tilde{\phi}\right)$ and **b** gain $(\tilde{P})$, $Re=7{,}400$

Experiments were carried out at wind velocities of $U_\infty=3$, 7 and 9 m/s, corresponding to $Re=3{,}200$, 7,400 and 9,500 and vortex shedding frequencies $f_s=24.6$, 57.4 and 73.8 Hz, respectively. The control performance was monitored using various measurement techniques. The LIF flow visualisation and PIV measurements were conducted using a Dantec standard PIV2100 system, including a CCD camera for digital particle images and two New Wave standard pulsed laser sources for illumination. Each image covered an area of 213×161 mm or $x/h\approx0$–13.2 and $y/h\approx-5$ to 5 of the flow field for LIF flow visualisation and 113×105 mm, i.e. $x/h\approx1$–8, $y/h\approx-2.9$–3.6, for PIV measurements. A two-component LDA system was used to measure the cross-flow distributions of fluctuating velocities and Reynolds shear stress at $x/h=3$. Readers may refer to Zhang et al. (2003) for more details of the PIV and LDA measurements.

The fluctuating lift and drag forces, F_L and F_D, were measured using two three-component load cells (Kistler 9251A) mounted at the two ends of the cylinder. The force capacity and sensitivity of the load cell were 5 kN and 8 pC/N, respectively. Hot wire B, made of 5-μm tungsten wire, was placed at $x/h=2$, $y/h=1.5$ and $z/h=4$ to monitor the change in flow velocity (u_2) under the control effect. The perturbation displacement (Y_p) was measured by a laser vibrometer, simultaneously with u_2 or F_L and F_D. The measurement uncertainty of the laser vibrometer was about 0.5%. The Y_p and u_2 signals, along with F_L and F_D, were conditioned and digitised using a 12-bit A/D board at a sampling frequency of 3.5 kHz per channel. The duration of each recording was 20 s.

3 Controller design and parameter tuning

The PID controller is simple and robust, which finds uses in many applications, such as process control and commercial controller hardware. The development and implementation of the PID controller was performed using an open source software platform, dSPACE. Using this platform, development processes such as real-time systems for rapid control prototyping, production code generation and hardware-in-the-loop tests were greatly simplified. A DSP, combining the SIMULINK function of MATLAB 6.1 with development software ControlDesk 2.0, was used for sampling and processing the feedback signal. By properly tuning the proportional gain (P), integral gain (I) and differential gain (D) of the PID controller, Zhang et al. (2004a, 2004b) successfully applied the system for the control of the resonant fluid–structure interaction. The tuning process was, however, tedious and time-consuming due to many combinations of P, I and D. In order to simplify the whole process, a two-parameter controller was developed through introducing a gain coefficient in amplitude $\tilde{P}$ and a phase shift $\tilde{\phi}$ between the output and input of the controller. Based on the transfer function of the PID controller (Franklin

et al. 1991), the simplified controller and the conventional PID controller are related by the following equations:

$$\tilde{P} = \sqrt{P^2 + \left(\frac{4\pi^2 D f_s^2 - I}{2\pi f_s}\right)^2} \quad (1)$$

$$\tilde{\phi} = \sqrt{\frac{4\pi^2 f_s^2 D - I}{2\pi f_s P}} \quad (2)$$

where f_s is the vortex shedding frequency. Both $\tilde{P}$ and $\tilde{\phi}$ should be adjusted during tuning.

Tuning the controller parameters was carried out for $U_\infty = 7$ m/s ($Re = 7{,}400$). Figure 2a shows the variation in the root mean square (rms) value, $u_{2,\mathrm{rms}}$, of u_2 from hot wire B for one cycle of $\tilde{\phi}$ as $\tilde{P}$ is kept constant at 0.3, 1 and 3, respectively. U_∞ is used to normalise $u_{2,\mathrm{rms}}$. When the paper was first submitted, $u_{2,\mathrm{rms}}$ was about 0.26, 0.27 and 0.253 at $\tilde{P} = 0.3$ and $\tilde{\phi} = 252°, 288°$ and 324°, respectively. These values were subsequently found incorrect and were changed to 0.28, 0.31 and 0.27, respectively, in the revision. It is noted that, for all $\tilde{P}$ values, $u_{2,\mathrm{rms}}$ displays its minimum at $\tilde{\phi} = 108°$ and reaches its maximum at $\tilde{\phi} = 288°$, suggesting a 180° phase shift between the two extremes. The results in Fig. 2a suggest that the open-loop perturbation at low amplitude (such as $\tilde{P} = 0.3$) may completely or partially suppress the vortex street, as long as the open-loop forcing does not lock-on to the vortex street (i.e. $\tilde{\phi} = 288°$). Open-loop control using different perturbation frequencies and amplitudes has been reported by Cheng et al. (2003). That work reported the dependence of the control performance on the perturbation amplitude (A_p) and frequency (f_p). When f_p is outside the lock-on range, structural vibration and vortex strength are suppressed. On the other hand, both structural vibration and the fluid field are enhanced as f_p falls within the lock-on range. The control performance is improved with the use of higher perturbation amplitudes A_p.

Figure 2b shows $u_{2,\mathrm{rms}}$ at $\tilde{\phi} = 108°$ and 288°, measured as $\tilde{P}$ varies from 0 to 9. At $\tilde{\phi} = 108°$, $u_{2,\mathrm{rms}}$ exhibits a dip at $\tilde{P} = 0.3$, a 40% fall compared to the unperturbed case (the dashed line). On the other hand, $u_{2,\mathrm{rms}}$ is persistently enhanced at $\tilde{\phi} = 288°$ and achieves a 90% amplification at $\tilde{P} = 9$ compared with the unperturbed condition. In following discussions, the two extremes, i.e. with the combinations of $\tilde{P} = 0.3$, $\tilde{\phi} = 108°$ and $\tilde{P} = 9$, $\tilde{\phi} = 288°$, are referred to as the impaired and the enhanced cases, respectively.

4 Performance of the closed-loop control

4.1 Flow modifications

Investigation was first conducted at $Re = 7{,}400$. Figure 3 shows the typical signals of u_2 and fluctuating lift and drag coefficients (C_L and C_D) when the closed-loop control was switched on and off. C_L and C_D are given by $F_L/(0.5\rho U_\infty^2 hl)$ and $F_D/(0.5\rho U_\infty^2 hl)$, respectively, where ρ and l stand for the air density and cylinder length, respectively. Without perturbation, the rms values of C_L and C_D are about 1.41 and 0.132, respectively, which are consistent with the values reported by Sakamoto et al. (1989). Evidently, the closed-loop-controlled perturbation has a great influence on all the signals, drastically reducing at $\tilde{P} = 0.3$ and $\tilde{\phi} = 108°$ (Fig. 3a) or amplifying at $\tilde{P} = 9$ and $\tilde{\phi} = 288°$ (Fig. 3b) their amplitudes. The variation is well reflected in the power spectral

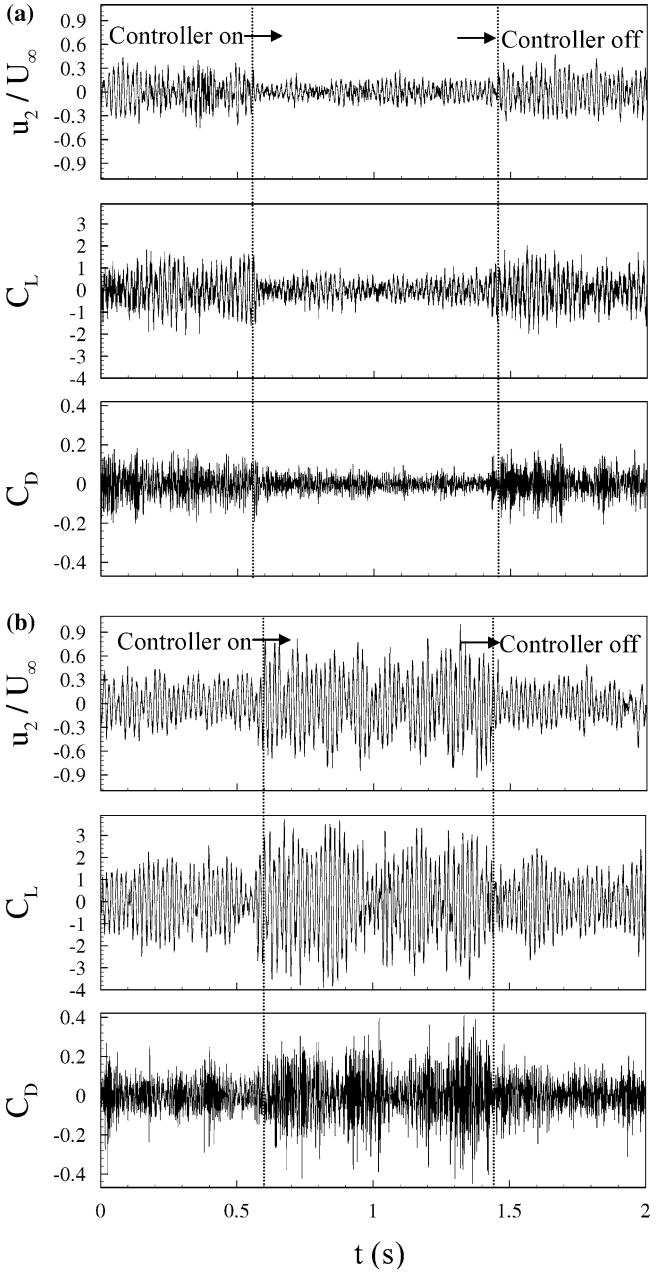

Fig. 3 Typical time histories of normalised fluctuating flow velocity (u_2), lift coefficient (C_L) and drag coefficient (C_D) when the controller was switched on and off: **a** impaired, **b** enhanced. $Re = 7{,}400$. Time is arbitrary

density functions, E_{u_2}, E_{F_L} and E_{F_D},of u_2, F_L and F_D (Fig. 4). The spectrum has been normalised so that $\int_0^\infty E_\alpha(f)\mathrm{d}f = 1$ (α stands for u_2, F_L or F_D). In the absence of perturbation, both E_{u_2} and E_{F_L} display a pronounced peak at $f_s^* = 0.132$, which is agreeable with previous measurements (e.g. Vickery 1966; Lyn and Rodi 1994; Zhou and Antonia 1994b). As expected, the most prominent peak in E_{F_D} occurs at $2f_s^*$. The number near the most pronounced peak indicates the peak magnitude. This magnitude decreases by 33% in E_{u_2},33% in E_{F_L} and 28% in E_{F_D} for the impaired case, and increases by 73% in E_{u_2}, 60% in E_{F_L} and 52% in E_{F_D} for the enhanced case. Correspondingly, the rms values of C_L and C_D reduce by 51% and 42%, respectively, for the former, but increase by 60% and 67%, respectively, for the latter.

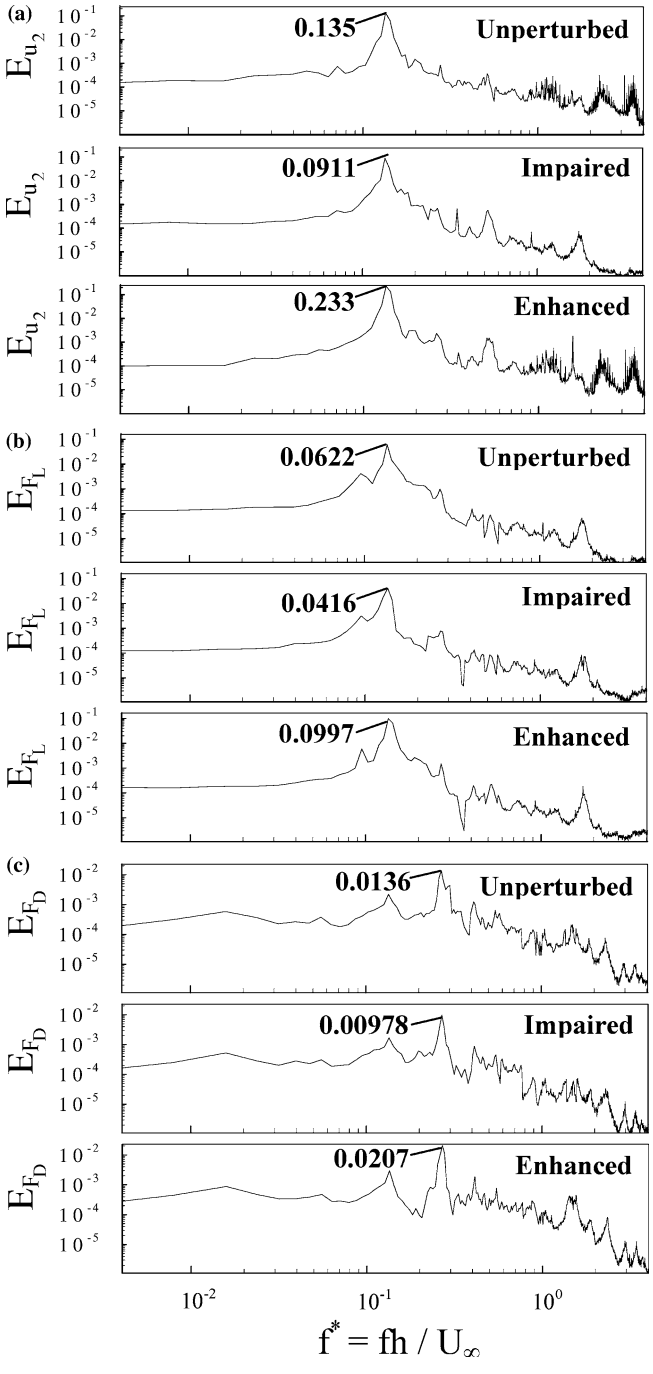

Fig. 4 The u_2, F_L and F_D spectra: **a** E_{u_2}; **b** E_{F_L}; **c** E_{F_D}. $Re = 7{,}400$

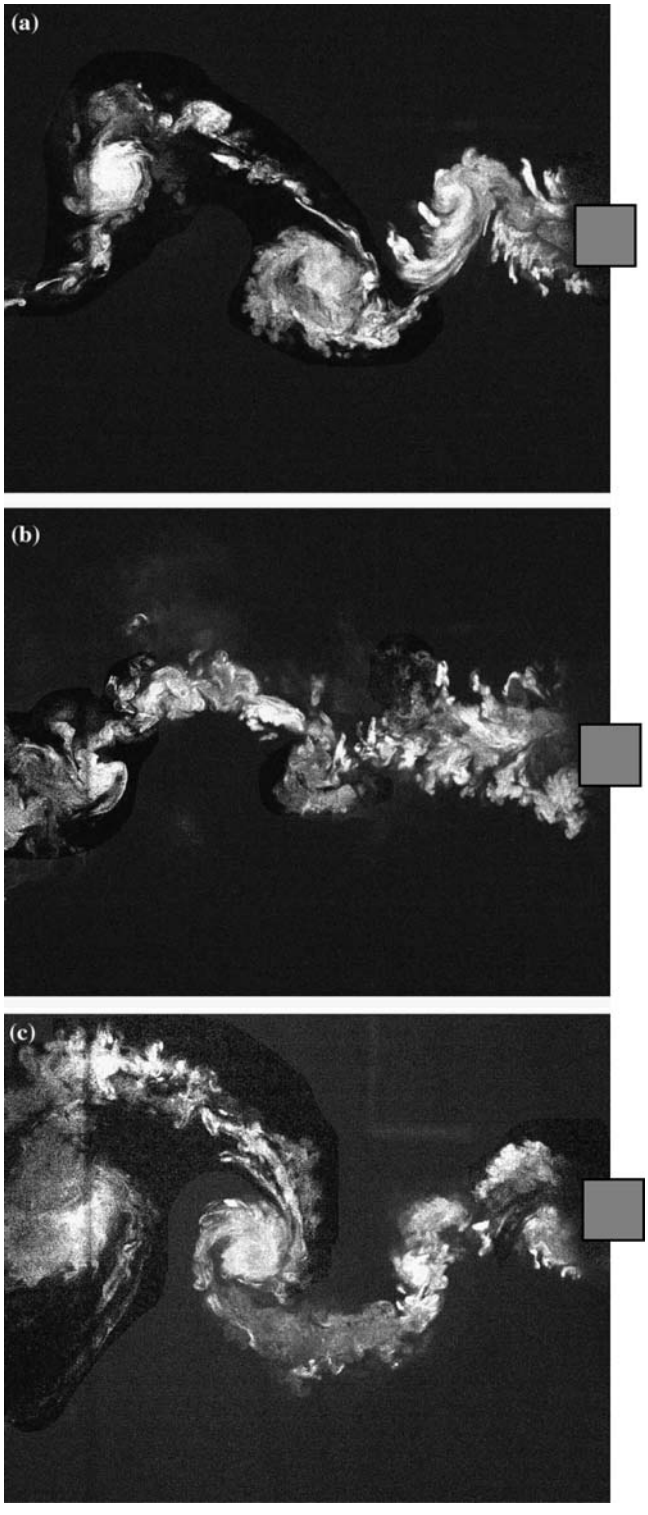

Fig. 5 Typical LIF flow visualisation photos: **a** unperturbed flow, **b** impaired, **c** enhanced. $Re = 7{,}400$

Figures 5 and 6 show the LIF flow visualisation photos and iso-contours of the normalised spanwise vorticity, $\omega_z^* = \omega_z h/U_\infty$, from the PIV measurement, respectively, for the unperturbed, impaired and enhanced cases. The square in the figures denotes the cylinder position. The maximum concentration of ω_z^* is given in Fig. 6, as is the cutoff level (0.3). The experimental uncertainty of ω_z^* was estimated to be about 9%. The Kármán vortex street is evident in Figs. 5a and 6a when perturbation is absent. This street is greatly impaired in Figs. 5b and 6b, and enhanced in Figs. 5c and 6c. The circulation (Γ) around a vortex is estimated by numerical integration: $\Gamma^* = \frac{\Gamma}{U_\infty h} = \sum_{i,j} \left(\omega_z^*\right)_{ij} \frac{\Delta A}{h^2}$ (Zhang et al. 2004b), where $\left(\omega_z^*\right)_{ij}$ is PIV-measured vorticity data over area $\Delta A = \Delta x \Delta y$, with Δx and Δy being the integral step along the x and y directions, respectively. Integration was conducted over an area enclosed by the cutoff level $\left|\omega_{zc}^*\right| = 0.3$, which is about 7% of $\left|\omega_{z\max}^*\right|$, the same as that used by Zhang et al. (2004b). The error associated with the Γ estimated was about 10%. The $\left|\omega_{z\max}^*\right|$ and Γ values drop by 50% and 71% for the impaired case and rise by 100% and 152% for the enhanced case, respectively, compared to the unperturbed flow. The results suggest an effective modification for vortex shedding.

Figure 7 presents the cross-flow distributions of the mean velocity $\overline{U}^*$ and Reynolds stresses $\overline{u^2}^*$, $\overline{v^2}^*$ and $\overline{uv}^*$ obtained from LDA measurements at $x/h = 3$. For the impaired case, the maximum $\overline{U}^*$, $\overline{u^2}^*$, $\overline{v^2}^*$ and $\overline{uv}^*$ exhibit a considerable decrease, down to 80%, 55%, 65% and 78% of their unperturbed counterparts, respectively. For the enhanced case, the quantities grow by 112%, 135%, 137% and 140%, respectively, compared to the unperturbed flow. The variations are expected in view of the significantly modified vortex strength. For instance, the impaired vortex strength is expected to reduce the entrainment of high-speed fluid from the free-stream to the wake, thus, causing an increased maximum velocity deficit and decreased fluctuating velocities (Warui and Fujisawa 1996; Williams et al. 1992). Interestingly, $\overline{uv}^*$ declines only marginally. In contrast, there is a considerable increase in $\overline{uv}^*$, as vortex shedding is enhanced (Fig. 7d). It is well established that the coherent structures in a turbulent near wake contribute little to the Reynolds shear stress; it is those relatively small-scale structures residing mostly in the saddle region between spanwise vortices that are responsible for the generation of the Reynolds shear stress (Zhou and Antonia 1994a). It will be shown later that the control mainly alters relatively large-scale structures in the wake for the impaired case, but it also affects flow structures across a wide range of frequencies, including those of relatively small scales. This explains the observation regarding $\overline{uv}^*$. From a different perspective, the vortex strength is doubled for the enhanced case. Subsequently, the straining motion of vortices is considerably enhanced in the saddle region, causing the appreciable rise in $\overline{uv}^*$ (Hussain and Hayakawa 1987).

The time-averaged drag coefficient, $\overline{C}_D$, may be estimated based on $\overline{U}^*$, $\overline{u^2}^*$ and $\overline{v^2}^*$ (Antonia and Rajagopalan 1990):

$$\overline{C}_D = 2\int_{-\infty}^{\infty} \frac{\overline{U}}{U_\infty}\left(\frac{U_\infty - \overline{U}}{U_\infty}\right) d\left(\frac{y}{h}\right) + 2\int_{-\infty}^{\infty} \left(\frac{\overline{v^2} - \overline{u^2}}{U_\infty^2}\right) d\left(\frac{y}{h}\right) \quad (3)$$

$\overline{C}_D$ thus determined is 2.05, falling in the range 1.7–2.1 of previous reports (Lee 1975; Shimada and Ishihara 2002; Zhou and Antonia 1994b). The value decreases by 20% for the impaired case, but increases by 37% for the

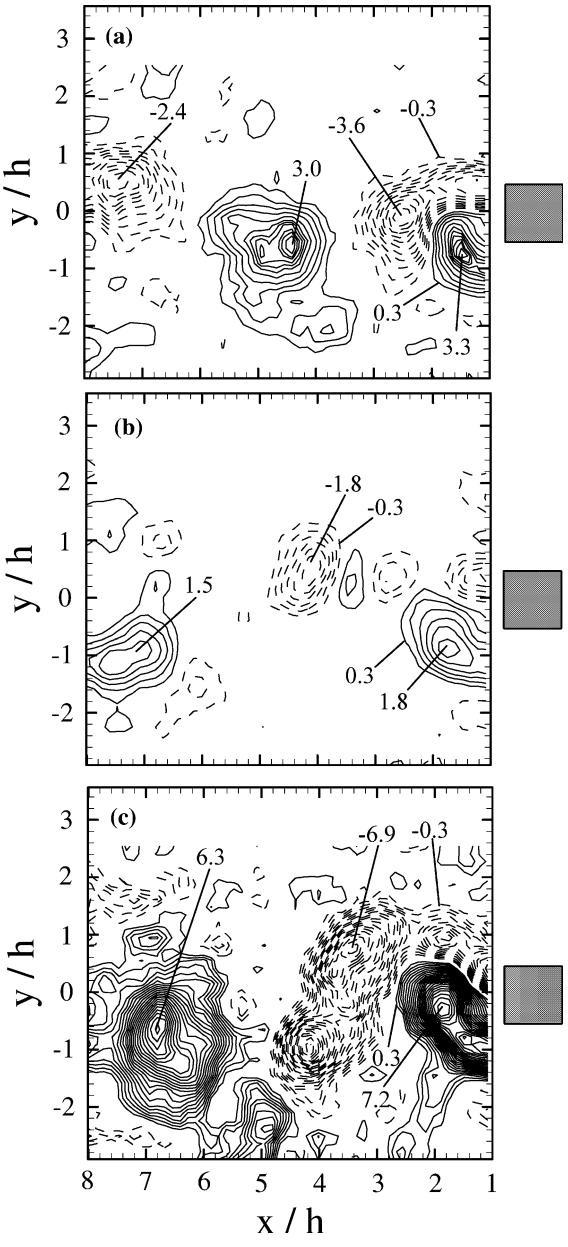

Fig. 6 Typical iso-contour of spanwise vorticity $\omega_z^* = \omega_z h/U_\infty$ from the PIV measurements: **a** unperturbed flow, **b** impaired, **c** enhanced. $Re = 7{,}400$

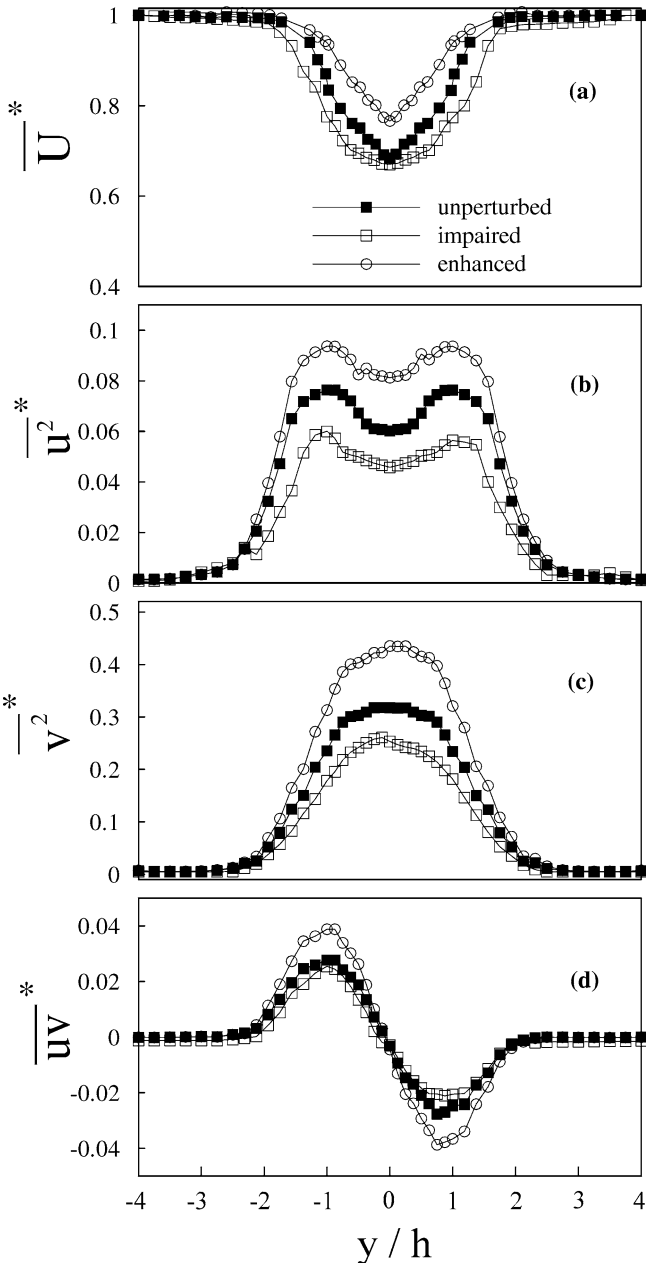

Fig. 7 Cross-flow distributions of mean velocity and Reynolds stresses at $x/h=3$: **a** $\overline{U}^*$; **b** $\overline{u^2}^*$; **c** $\overline{v^2}^*$; **d** $\overline{uv}^*$. $Re=7{,}400$

enhanced case. Fujisawa and Nakabayashi (2002) reduced $\overline{C}_D$ by 16% by using a rotating cylinder to control vortex shedding and attributed the effect to a diminished $\overline{u^2}^*$, which seems to be corroborated by the present data. A change in the near-wake fluctuation, as evidenced in $\overline{u^2}^*$ and $\overline{v^2}^*$, may have an impact upon flow separation and, hence, the backpressure, leading to a modified $\overline{C}_D$.

4.2 Robustness of the closed-loop control

The controller was presently tuned under the designed condition ($Re=7{,}400$) to provide optimum performance. Unlike an open-loop control system, the closed-loop control system is expected to possess a certain degree of robustness when the experimental conditions change. This feature is confirmed by applying the controller tuned at $Re=7{,}400$ to 3,200 and 9,500, respectively. Table 1 tabulates the variation in Γ, $u_{2,\mathrm{rms}}$, $C_{\mathrm{L,rms}}$ and $C_{\mathrm{D,rms}}$ (the rms values of C_L and C_D, respectively) for both impaired and enhanced cases for the three Reynolds numbers. In general, the flow is similarly modified by the closed-loop perturbation. It is not surprising to see that the best performance is obtained at $Re=7{,}400$. At $Re=3{,}200$ and 9,500, Γ reduces by 42% and 58%, respectively, for the impaired case, but rises by 92% and 120%, respectively, for the enhanced case, compared to the uncontrolled condition. The modified flow is also verified by the LIF photos and PIV data (not shown). The same observation is made for $u_{2,\mathrm{rms}}$, $C_{\mathrm{L,rms}}$ and $C_{\mathrm{D,rms}}$ for the three Reynolds numbers.

5 Discussions

Using a closed-loop control technique similar to the present one, Zhang et al. (2004b) observed an almost complete annihilation of the vortex street behind the resonating cylinder and vortex shedding. The observation was ascribed to the opposite movement between the cylinder and the lateral flow velocity associated with vortex shedding under the controlled perturbation. However, the present cylinder was rigid and fixed at both ends.

In order to explore the underlying physics of the present observation, the perturbation signal (Y_p) and the streamwise fluctuating velocity (u_2) from hot wire B were simultaneously measured, as were the fluctuating lift (C_L) and Y_p. The spectral phase shift, $\phi_{\alpha_1\alpha_2} \equiv \tan^{-1}(Q_{\alpha_1\alpha_2}/\mathrm{Co}_{\alpha_1\alpha_2})$, between α_1 and α_2, where $Q_{\alpha_1\alpha_2}$ and $\mathrm{Co}_{\alpha_1\alpha_2}$ are the quadrature spectrum and co-spectrum of α_1 and α_2, respectively, and α_1 and α_2 represent Y_p and u_2 or C_L and Y_p. See Bendat and Piersol (1993) for more details. The phase spectrum is computed from the Fourier transform of the correlation $\alpha_1(t+\tau)\alpha_2(t)$ (Zhang et al. 2000).

Figure 8 presents $\phi_{Y_p u_2}$ as f^* varies for the three Re values. At $Re=7{,}400$, $\phi_{Y_p u_2}$ is about $-\pi$ over a small range of frequencies around f_s^* for the impaired case, but zero across the whole range of frequencies for the enhanced case (Fig. 8a). An analysis similar to that by

Table 1 Control performance at different Re: variation in Γ, $u_{2,\mathrm{rms}}/U_\infty$, $C_{\mathrm{L,\,rms}}$ and $C_{\mathrm{D,\,rms}}$ compared to the unperturbed flow. ↓ and ↑ denote a decrease and increase, respectively

Re	7,400		3,200		9,500	
Γ	71%↓	152%↑	42%↓	92%↑	58%↓	120%↑
$u_{2,\mathrm{rms}}/U_\infty$	40%↓	90%↑	26%↓	55%↑	31%↓	56%↑
$C_{\mathrm{L,\,rms}}$	51%↓	60%↑	33%↓	30%↑	37%↓	51%↑
$C_{\mathrm{D,\,rms}}$	42%↓	67%↑	20%↓	13%↑	37%↓	48%↑

Cheng et al. (2003) points to the reasoning that $\phi_{Y_p u_2}$ is equivalent to the phase shift between the perturbation velocity $\dot{Y}_p$ of the cylinder surface and the lateral flow velocity component, v, around the cylinder. Therefore, $\phi_{Y_p u_2} = -\pi$ means anti-phased $\dot{Y}_p$ and v; that is, the surface perturbation created by actuators actually moves against the lateral flow velocity. This opposite movement between $\dot{Y}_p$ and v is responsible for the greatly impaired vortex shedding (Figs. 5b, 6b). Similarly, $\phi_{Y_p u_2} = 0$ corresponds to the in-phased $\dot{Y}_p$ and v, which promotes the roll-up motion of the vortices (Figs. 5c, 6c). The interrelationship between $\dot{Y}_p$ and v mimics the cylinder and fluid motions in Zhang et al. (2003, 2004b). Nonetheless, since the cylinder displacement in the investigation by Zhang et al. grossly exceeds Y_p, the opposite motion between the cylinder and the fluid produced a more dramatic effect, resulting in an almost complete destruction of the vortex street.

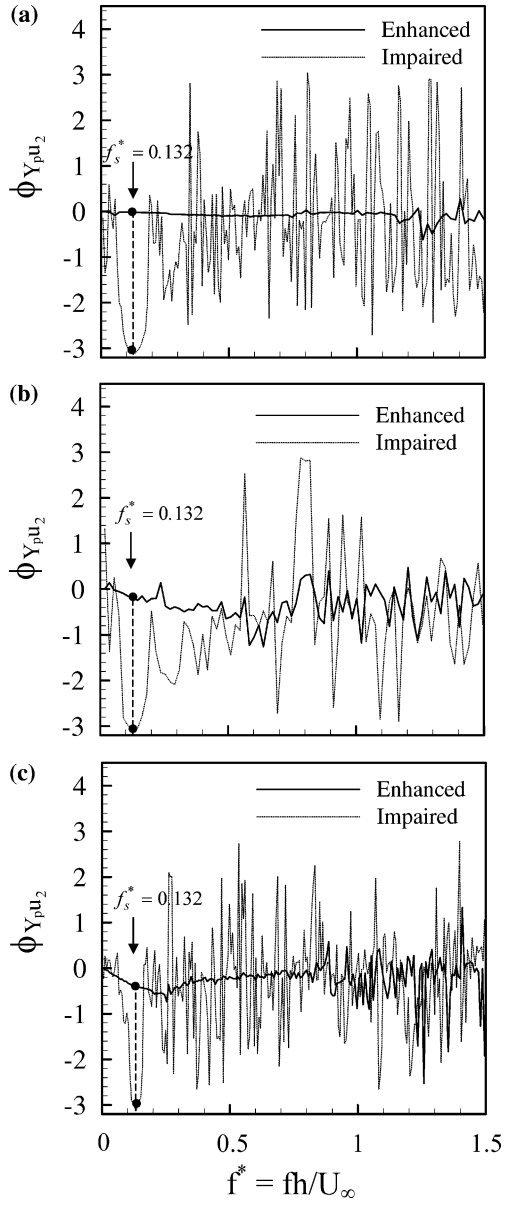

Fig. 8a–c Phase shift $\phi_{Y_p u_2}$ between Y_p and u_2: $Re =$ **a** 7,400; **b** 3,200; **c** 9,500

Interestingly, the perturbation results in the anti-phased $\dot{Y}_p$ and v over a small range of frequencies around f_s^* for the impaired case, but the synchronised $\dot{Y}_p$ and v across almost the entire frequency range for the enhanced case (Fig. 8). This explains why the enhancement impact appears to be overwhelming that of the impaired case (Figs. 2, 3, 4, 5, 6, 7). It may be inferred that the present control technique suits well the applications where it is desirable to enhance vortex shedding, such as vortex generators.

A spectral coherence between two signals, α_1 and α_2, is defined by $\mathrm{Coh}_{\alpha_1\alpha_2} = \left(\mathrm{Co}^2_{\alpha_1\alpha_2} + Q^2_{\alpha_1\alpha_2}\right)/.E_{\alpha_1}E_{\alpha_2}$, which provides a measure of the degree of correlation between the Fourier components of α_1 and α_2. $\mathrm{Coh}_{Y_p u_2}$ was computed for the above three Reynolds numbers. The maximum $\mathrm{Coh}_{Y_p u_2}$ occurs at f_s^* and does not exceed 0.11 for the impaired case, but increases almost across the entire frequency range, reaching the maximum (0.7) for the enhanced case (Fig. 9a).

Note that the perturbation was imposed only on the upper surface of the square cylinder. However, the vortices shed from both sides of the cylinder appear equally impaired or enhanced under the perturbation (Figs. 5, 6). Vortex shedding is a result of initial wake instability (Provansal et al. 1987). In order to form a stable vortex street, it is essential for the two oppositely signed vortices separating from the cylinder to have approximately the same strength through interactions (Sakamoto et al. 1991). In other words, if the vortex strength on one side decreases or increases, it will do so on the other side to counterbalance this change, and vice versa. Therefore, vortex shedding from both sides of the cylinder appears equally affected, notwithstanding the perturbation only on one side.

As Re is varied, the interrelationship between $\dot{Y}_p$ and v largely remains unchanged. Nevertheless, the frequency range over which $\dot{Y}_p$ and v are anti-phased narrows slightly for the impaired case (Fig. 8b, c) or $\phi_{Y_p u_2}$ may slightly deviate from zero or fluctuate about zero at some frequencies for the enhanced case, which is agreeable with corresponding $\mathrm{Coh}_{Y_p u_2}$ (Fig. 9b, c).

Insight into the physics of the present flow control may be better gained by investigating the force interaction between the perturbed surface and the flow. The behaviour of $\phi_{Y_p C_L}$ (Fig. 10) is rather similar to $\phi_{Y_p u_2}$: $\phi_{Y_p C_L}$ is about zero for the enhanced case, but $-\pi$ for the impaired case, and undergoes changes similar to $\phi_{Y_p u_2}$ for different Re. $\mathrm{Coh}_{Y_p C_L}$ also exhibits a change similar to $\mathrm{Coh}_{Y_p u_2}$ (Fig. 11). The fluctuating lift force F_L on the cylinder, measured by the load cell, is largely attributed to the alternate separation of the boundary layer from the cylinder. This force is equal in magnitude and opposite in direction or anti-phased to the force, F'_L, of the cylinder acting on fluid. Using a moving cylinder in a cross flow, Lighthill (1986) and Williamson (1985)

decomposed F'_L into a "vortex force" component F_f, due to vortex shedding, and a "potential force" component $F_{potential}$, caused by the potential added mass force. The latter could be estimated by $F_{potential} = -(C_A m_d \ddot{Y})$. Here, C_A, m_d and $\ddot{Y}$ represent the ideal added mass (=1.0), displaced fluid mass ($=\pi\rho h^2 l/4$, where ρ is the fluid density and l is the cylinder length) and lateral acceleration of the cylinder oscillation, respectively (Govardhan and Williamson 2000). $F_{potential}$ presently corresponds to F_p generated due to the introduction of a perturbation. The three force vectors satisfy the relation $\overrightarrow{F'_L} = \overrightarrow{F_f} + \overrightarrow{F_p}$. F_p is directly proportional to the acceleration of fluid on the perturbed surface, which is anti-phased to Y_p. The same phase shift (π) from F_L (or C_L) to F'_L as from Y_p to F_p implies that $\phi_{Y_pC_L}$ reflects the phase relation between F_p and F'_L. Note that F_f overwhelms F_p in view of the very small perturbation amplitude; that is, F_f and F'_L are approximately in-phase. Therefore, the phase relation between F_p and F'_L in fact reflects that between F_p and F_f. We may now piece together the picture of the perturbed flow. The relation $\phi_{Y_pC_L} = 0$ corresponds to in-phased F_f and F_p, leading to an amplified F'_L and enhancing vortex shedding. On the other hand, $\phi_{Y_pC_L} = -\pi$ corresponds to anti-phased F_f and F_p, resulting in a reduced F'_L and impaired vortex shedding.

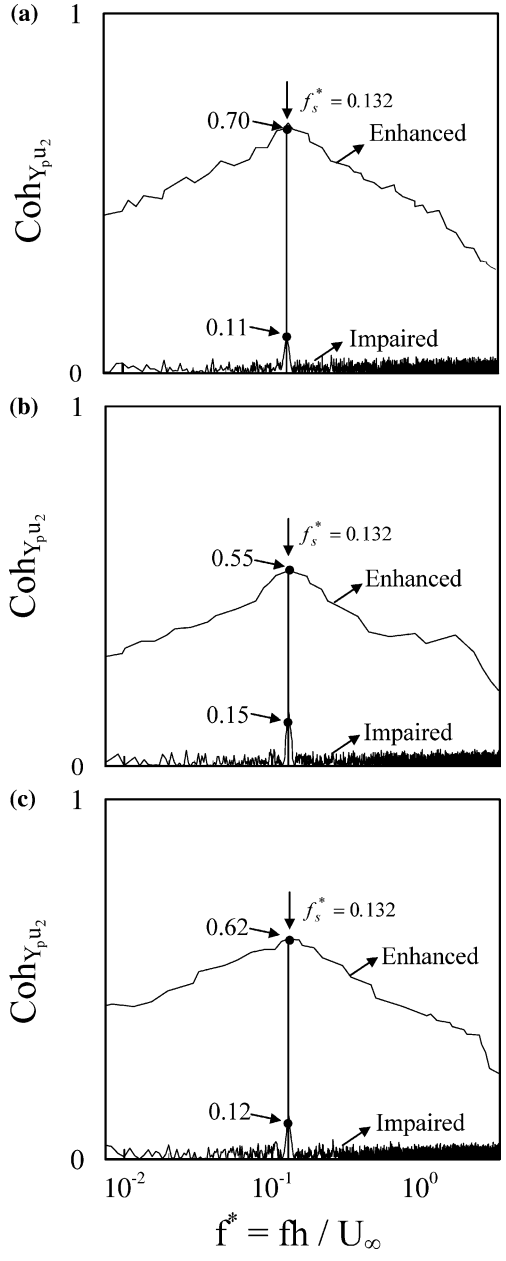

Fig. 9 Spectral coherence $Coh_{Y_pu_2}$ between perturbation signal (Y_p) and u_2: $Re =$ **a** 7,400; **b** 3,200; **c** 9,500

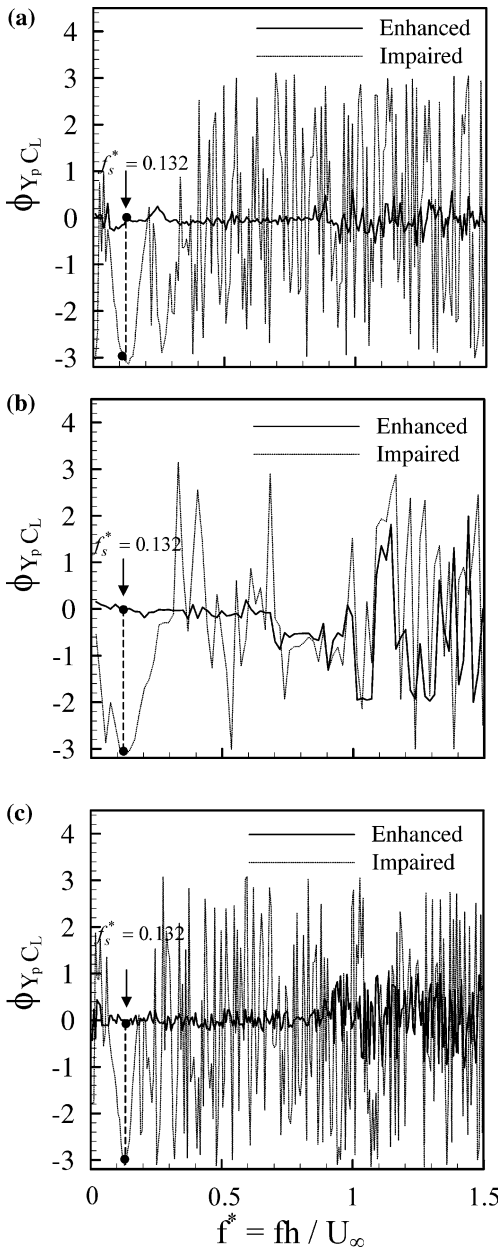

Fig. 10 Phase shift $\phi_{Y_pC_L}$ between perturbation signal (Y_p) and the fluctuating lift coefficient signal (C_L): $Re =$ **a** 7,400; **b** 3,200; **c** 9,500

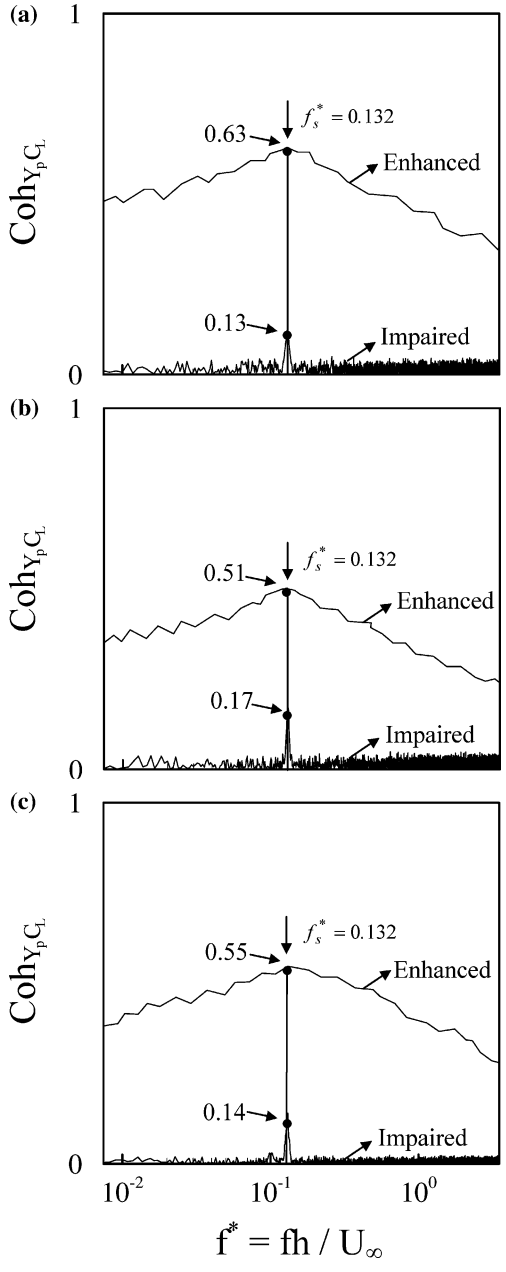

Fig. 11 Spectral coherence $Coh_{Y_pC_L}$ between perturbation signal (Y_p) and C_L: $Re =$ **a** 7,400; **b** 3,200; **c** 9,500

6 Conclusions

Experimental investigation has been conducted to control the turbulent wake of a fixed square cylinder. Control was made possible by perturbing one cylinder surface using piezo-ceramic actuators, which are activated on feedback fluctuating flow velocity. The investigation leads to following conclusions:

1. The proposed technique is effective in either suppressing or enhancing the vortex street behind the cylinder. The interrelationship is crucial between the surface perturbation force, F_p, and the force, F_f, of the cylinder acting on the fluid that is associated with vortex shedding. When the two forces are anti-phased, vortex shedding is greatly weakened. The vortex strength, fluctuating lift and drag coefficients drop by 71%, 51% and 42%, respectively. The mean drag coefficient decreases by 20%. When in-phased, F_p and F_f re-enforce each other, which enhances significantly vortex shedding. Consequently, the vortex strength increases by 152%, the fluctuating lift and drag coefficients experience a great jump, and the mean drag coefficient rises by 37%.
2. Tuned under one Reynolds number, the proposed technique is demonstrated to be effective over a range of Reynolds numbers.
3. The present one-sided perturbation has the same effect on vortices shed from both sides of the cylinder, thus, producing a reasonably symmetrical wake about the centreline.

It is worth pointing out that the cross-section of the cylinder is presently chosen to be square only for the convenient installation of actuators. The present technique should be effective to control the wakes of cylinders with other cross-sections.

Acknowledgements The authors wish to acknowledge the support given to them by the Research Grants Committee of The HKSAR (grant no. PolyU 5294/03E).

References

Antonia RA, Rajagopalan S (1990) A comment on the determination of drag of a circular cylinder. AIAA J 28:1833–1835

Baz A, Ro J (1991) Active control of flow-induced vibrations of a flexible cylinder using direct velocity feedback. J Sound Vib 146:33–45

Bendat JS, Piersol AG (1993) Engineering applications of correlation and spectral analysis, 2nd edn. Wiley, New York

Berger E (1967) Suppression of vortex shedding and turbulence behind oscillating cylinders. Phys Fluids 10:191–193

Cheng L, Zhou Y, Zhang MM (2003) Perturbed interaction between vortex shedding and induced vibration. J Fluid Struct 17:887–901

Franklin Gere F, David Powell J, Emami-Naeini A (1991) Feedback control of dynamics systems, 2nd edn. Addison-Wesley, California, pp 107–147

Fujisawa N, Nakabayashi T (2002) Neural network control of vortex shedding from a circular cylinder using rotational feedback oscillations. J Fluid Struct 16(1):113–119

Gad-el-Hak M (2001) Flow control: the future. J Aircraft 38:402–418

Govardhan R, Williamson CHK (2000) Modes of vortex formation and frequency response for a freely vibrating cylinder. J Fluid Mech 420:85–130

Huang XY (1996) Feedback control of vortex shedding from a circular cylinder. Exp Fluids 20:218–224

Hussain AKMF, Hayakawa M (1987) Eduction of large-scale organized structures in a turbulent plane wake. J Fluid Mech 180:193–229

Lee BE (1975) The effect of turbulence on the surface pressure field of a square prism. J Fluid Mech 69:263–282

Lighthill J (1986) Fundamentals concerning wave loading on offshore structures. J Fluid Mech 173:667–681

Lyn DA, Rodi W (1994) The flapping shear layer formed by flow separation from the forward corner of a square cylinder. J Fluid Mech 267:353–376

Marouzé JP, Cheng L (2002) A feasibility study of active vibration isolation using THUNDER actuators. Smart Mater Struct 11:854–862

Provansal M, Mathis C, Boyer L (1987) Benard-von Kármán instability: transient and forced regimes. J Fluid Mech 182:1–22

Roussopoulos K (1993) Feedback control of vortex shedding at low Reynolds numbers. J Fluid Mech 248:267–296

Sakamoto H, Haniu H, Kobayashi Y (1989) Fluctuating force acting on rectangular cylinders in uniform flow (on rectangular cylinders with fully separated flow). Trans Jpn Soc Mech Eng Ser B 55(516):2310–2317

Sakamoto H, Tan K, Haniu H (1991) An optimum suppression of fluid forces by controlling a shear layer separated from a square prism. J Fluids Eng 113:183–189

Shimada K, Ishihara T (2002) Application of a modified k-ε model to the prediction of aerodynamic characteristics of rectangular cross section cylinders. J Fluid Struct 16(4):465–485

Tokumaru PT, Dimotakis PE (1991) Rotary oscillation control of a cylinder wake. J Fluid Mech 224:77–90

Tsutsui T, Igarashi T, Nakamura H (2001) Drag reduction and heat transfer enhancement of a square prism. JSME Int J B Fluid Thermal Eng 44:575–583

Turner JT, Popiel CO, Robinson DI (1993) Evolution of an improved vortex generator. Flow Meas Instrum 4:249–258

Vickery BJ (1966) Fluctuating lift and drag on a long cylinder of square cross-section in a smooth and turbulent stream. J Fluid Mech 25:481–494

Wang Y, Haller G, Banaszuk A, Tadmor G (2003) Closed-loop Lagrangian separation control in a bluff body shear flow model. Phys Fluids 15:2251–2266

Warui HM, Fujisawa N (1996) Feedback control of vortex shedding from a circular cylinder by cross-flow cylinder oscillations. Exp Fluids 21:49–56

Williams JEF, Zhao BC (1989) The active control of vortex shedding. J Fluid Struct 3:115–122

Williams DR, Mansy H, Amato C (1992) The response and symmetry properties of a cylindrical wake subjected to localized surface excitation. J Fluid Mech 234:71–96

Williamson CHK (1985) Sinusoidal flow relative to circular cylinders. J Fluid Mech 155:141–174

Zhang HJ, Zhou Y, Antonia RA (2000) Longitudinal and spanwise structures in a turbulent wake. Phys Fluids 12:2954–2964

Zhang MM, Zhou Y, Cheng L (2003) Spring-supported cylinder wake control. AIAA J 41:1500–1506

Zhang MM, Cheng L, Zhou Y (2004a) Closed-loop control of fluid–structure interactions on a flexibly supported cylinder. EUR J Mech B—Fluid 23:187–197

Zhang MM, Cheng L, Zhou Y (2004b) Closed-loop-controlled vortex shedding from a flexibly supported cylinder under different schemes. Phys Fluids 16:1439–1448

Zhou Y, Antonia RA (1994a) Critical points in a turbulent near-wake. J Fluid Mech 275:59–81

Zhou Y, Antonia RA (1994b) Effect of initial conditions on structures in a turbulent near-wake. AIAA J 32:1207–1213

Zhou Y, Zhang HJ, Yiu MW (2002) The turbulent wake of two side-by-side circular cylinders. J Fluid Mech 458:303–332